Mechanistic Significance of the Preparatory Migration of Hydrogen Atoms around the FeMo-co Active Site of Nitrogenase†

Ian Dance*

School of Chemistry, University of New South Wales, Sydney, NSW 2052, Australia

Received October 31, 2005; Revised Manuscript Received January 31, 2006

ABSTRACT: The migration of H atoms over S and Fe atoms in the reaction domain of FeMo-co, the active site of nitrogenase, is described and used to explain mechanistic data on the catalyzed reductions of N_2 and C_2H_2. After electron transfer to FeMo-co, H atoms are generated by fast proton supply to S3B (atom labels from structure 1M1N) and migrate vectorially via several pathways from S3B to locations on the FeMo-co face, specifically Fe6, S2B, Fe2, and S2A (calculated reaction profiles are reported). The E_nH_n reduction levels ($n = 1-4$) in the Thorneley−Lowe kinetic-mechanistic schemes are each potential sequences of substructures with different distributions of H atoms. The positions of H atoms influence the binding of substrates N_2 and C_2H_2, and the bound substrate subsequently blocks further migration of H atoms past the binding site. This model provides a consistent structural interpretation of (a) the two-site reactivity of C_2H_2 and the differentiation of the high- and low-affinity sites as due to different preparatory H migration; (b) the differing mutual inhibitions of N_2 and C_2H_2 in wild-type protein; (c) the modified reactivity of the *Azotobacter vinelandii* α-$^{Gly}69^{Ser}$ mutant with N_2 and C_2H_2; and (d) the basis for the stereoselectivity of hydrogenation of C_2D_2 and its loss in some mutant proteins. Some structures for initially bound N_2 and C_2H_2, and their hydrogenated intermediates, are presented. The key new concept is that binding sites and binding states for substrates and intermediates are characterized not only by their locations on the FeMo-co face but also by the structural and temporal status of the distribution of H atoms over the FeMo-co reaction domain.

Nitrogenase is the enzyme that reduces atmospheric N_2 to ammonia, providing the natural source of reduced nitrogen for the sustenance of life in the biosphere, according to the idealized stoichiometry of eq 1.

$$N_2 + 8H^+ + 8e^- + 16ATP \rightarrow 2NH_3 + H_2 + 16ADP + 16P_i \quad (1)$$

Two metalloproteins are involved: the Fe-protein couples ATP hydrolysis with electron transfer to the MoFe protein, which contains the FeMo-cofactor (FeMo-co[1]), the site of reduction of N_2 (and other substrates) (*1*−*9*). Although the biochemical mechanism involving the associations and dissociations of the two component proteins is fairly well understood, the chemical mechanism for the catalyzed reduction of N_2 is still largely unknown at the atomic/structural level (*7*, *10*−*15*).

The FeMo-co active site is an $N^cFe_7MoS_9$(homocitrate) cluster (Figure 1), linked to the surrounding protein by a cysteine residue at Fe1 and a histidine residue at Mo. There is no direct evidence for the identity of the central atom labeled N^c (*15*−*17*), here assumed to be nitrogen; the consequences of it being carbon, the only other likely possibility (*18*−*20*), are discussed at the end of this article. FeMo-co contains six μ_3-S and three μ-S ligands. Investigations using site-directed mutagenesis have established that the face of FeMo-co containing atoms Fe2, Fe3, Fe6, and Fe7 linked by S2A, S2B, S3B, and S5A is the most probable site of reaction. Significant recent progress has flowed from investigations of MoFe proteins with alternative residues at position α-70 (*21*−*23*), permitting the trapping and spectroscopic measurement of intermediates containing allyl alcohol and allylamine (*24*, *25*), hydride (*26*), nitrogen (*27*), and hydrazine (*27*, *28*) and strongly implicating Fe2 and Fe6 as the catalytic sites (*29*, *30*).

A key mechanistic tenet, evolving from the interpretation of the comprehensive kinetic data of Thorneley and Lowe (*10*, *31*−*34*), is that the resting state E_0 of FeMo-co is reduced in $e^- + H^+$ steps through a series of hydrogenated intermediates E_1H_1, E_2H_2, E_3H_3, and E_4H_4. In the previous article (*35*), I showed that electronation of FeMo-co causes its S atoms to become more basic, and that protons can be introduced along well-defined specific chains of water molecules through the surrounding protein, terminating at water molecule 679 (Figure 1). This electronation of FeMo-co plus the protonation of S3B via HOH679 generates an H atom bound to S3B that can move to other Fe and S atoms of FeMo-co. The E_nH_n levels are described in terms of H atoms bound to the S and Fe atoms of FeMo-co.

† This research is supported by the Australian Partnership for Advanced Computing, the University of New South Wales, and the Australian Research Council.

* To whom correspondence should be addressed. Phone: 612 9415 8404. Email: i.dance@unsw.edu.au.

[1] Abbreviations: FeMo-co, FeMo cofactor of the MoFe protein of nitrogenase; *Av*, *Azotobacter vinelandii*; *Kp*, *Klebsiella pneumoniae*; *Cp*, *Clostridium pasteurianum*; WT, wild type; K_m, Michaelis constant; V_{max}, maximum rate for Michaelis−Menten enzyme kinetics; HOMO, highest occupied molecular orbital; LUMO, lowest unoccupied molecular orbital; TS, transition state.

10.1021/bi052217h CCC: $33.50
Published on Web 04/28/2006

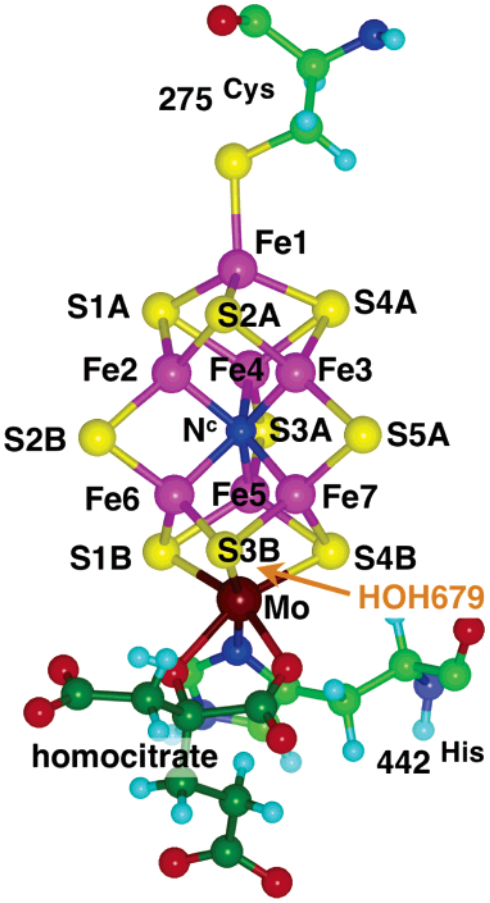

FIGURE 1: Structure of FeMo-co connected to the protein via α-275^{Cys} and α-442^{His} (*Azotobacter vinelandii*), with atom labeling for the crystal structure 1M1N. The C atoms of homocitrate are dark green. The location of the key water molecule HOH679 and the direction of its proton transfer to S3B are marked in orange.

Although N_2 is the physiological (and most enigmatic) substrate, acetylene is a significant alternative substrate for a number of reasons. First, it is rapidly reduced by nitrogenase to ethylene and has long been used for the practical assay of nitrogenase activity. Second, it has the potential to monitor the cis/trans stereochemistry of addition, and the hydrogenation of C_2D_2 to form cis or trans $C_2H_2D_2$ has been reported for wild-type and mutant enzymes (*36*−*39*). These stereochemical data about the mechanism of reaction are not provided by N_2 or any other substrates except other alkynes and cyclopropene (*2*, *8*). Third, there is substantial kinetic data on the mutually inhibitory interactions of C_2H_2 and N_2. As will become evident, it is significant that C_2H_2 requires only two reduction equivalents, whereas N_2 requires six.

Thorneley and Lowe developed reaction schemes for N_2 (Scheme 1) (*10*) and C_2H_2 (Scheme 2) (*40*) to account for the kinetic data. The progression of reduction levels E_1H_1, E_2H_2, E_3H_3, and E_4H_4 of FeMo-co and the possibilities for hydrogen production, $E_nH_n \rightarrow E_{n-2}H_{n-2} + H_2$, are common to both schemes. Productive involvement of N_2 does not occur until the E_3H_3 reduction level has been reached (Scheme 1), but productive involvement of C_2H_2 begins at the E_1H_1 level. (There is evidence that C_2H_2 binds to resting state E_0 (*41*), but this does not lead to the product.) Note also that the initial binding of N_2 is believed to involve the substitution of H_2 (Scheme 1), whereas the binding of C_2H_2 does not. Scheme 1 also accounts for the inhibition of N_2 reduction by H_2 and the limiting stoichiometry of one H_2 released per N_2 reduced (eq 1) and has been elaborated to account for another informative reaction of nitrogenase, the N_2-dependent reduction of D_2 to 2HD (*10*, *11*, *33*, *35*).

The use of N_2 and C_2H_2 as cosubstrates has led to valuable data on their mutual interactions. In the wild-type enzyme, N_2 is a weak competitive inhibitor of C_2H_2 reduction, but C_2H_2 is an effective noncompetitive inhibitor of N_2 reduction (*36*, *42*, *43*). This behavior changes in the *Av* $^{Gly}69^{Ser}$ mutant, which has diminished C_2H_2 activity (but essentially unchanged N_2 and H^+ activity), and the inhibition of N_2 activity by C_2H_2 is competitive in contrast to the noncompetitive inhibition of wild-type protein (*44*, *45*). The *Av* $^{His}195^{Gln}$ mutant is unable to reduce N_2, but N_2 is a competitive inhibitor of C_2H_2 reduction (*46*), indicating that N_2 is still binding, but unproductively.

Scheme 1: Modified Presentation of the Thorneley−Lowe Scheme to Account for the Kinetics of Nitrogenase (*10*)[a]

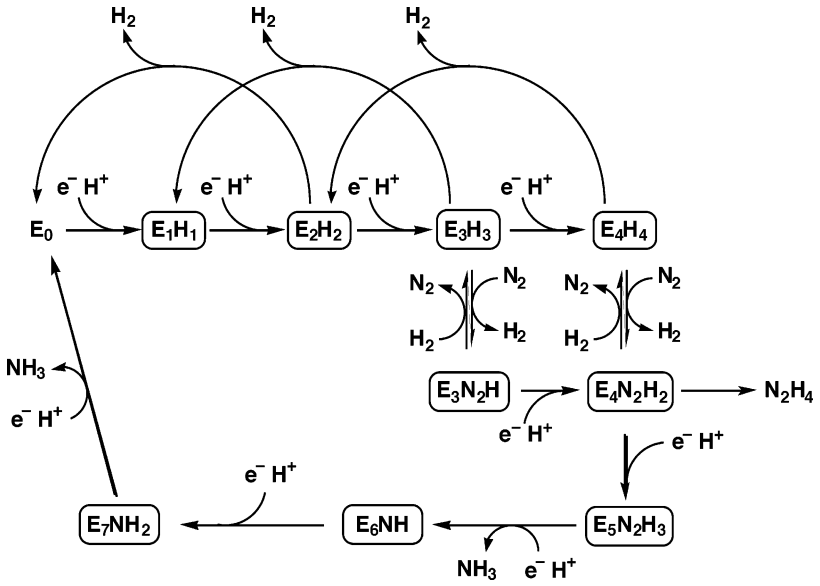

[a] The formulas of the intermediates that are enclosed signify only composition.

Scheme 2: Thorneley−Lowe Scheme for the Reduction of Acetylene (*40*)[a]

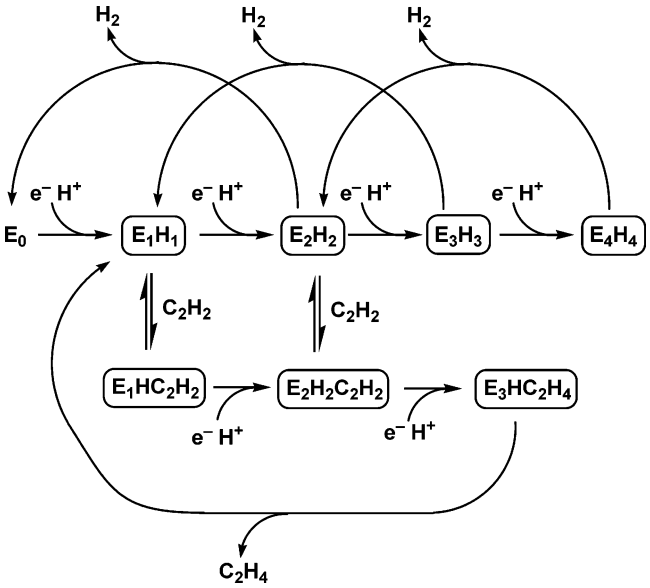

[a] The formulas of the intermediates that are enclosed signify only composition.

A two-site model for the reactions of C_2H_2 has developed from a number of observations. EPR signal intensities for *Kp* turning over under variable C_2H_2 concentration were interpreted in terms of tight and loose binding sites with K_m values differing by ca. 10^3 (*47*). The kinetic behavior of *Cp* with C_2H_2 was analyzed in terms of high-affinity and low-affinity pathways, with K_m values of 0.003 and 0.23 atm, respectively (*48*). Many kinetic and stereochemical properties of *Av* reacting with C_2D_2 provide evidence for high- and low-affinity binding sites (*39*). Results from modified proteins also support dual pathways for C_2H_2. In *Av* $^{Gly}69^{Ser}$ the high-affinity pathway is disabled but low-affinity reactivity with C_2H_2 (K_m 0.14 atm) is retained, with V_{max} and the inhibition by N_2 and CO unchanged from the wild-type behavior, leading to the proposal that the reactivity of the $^{Gly}69^{Ser}$ protein is that of the low-affinity site and that the reaction through the high-affinity site has been blocked in the mutant (*44*). Indirect evidence for two close reaction sites for C_2H_2 came from kinetic data on the partial inhibition by CO in the $^{Arg}277^{His}$ mutant (*49*).

The objective of this article is to develop a structural mechanistic model for the early stages of the reactions of N_2 and C_2H_2, that is, a model that accounts for the data outlined in the preceding introduction, and particularly the high- and low-affinity pathways for C_2H_2 and the mutually inhibitory reactivity patterns in the wild-type and mutant enzymes. This model builds on the general description of the hydrogen chemistry of FeMo-co (*35*) in which a proton supply chain terminating in a water molecule 679 generates a hydrogen atom on S3B during each reduction cycle: $E_nH_n \rightarrow E_{n+1}H_{n+1}$. The migration of H atoms from S3B to the other atoms of the reaction zone, namely, Fe6, S2B, Fe2, and S2A, is a crucial component of the explanations. To develop the model, it is necessary to provide some information about the binding modes of N_2 and C_2H_2 to FeMo-co. Density functional calculations are used to obtain structures and determine reaction barriers.

The terms used to describe processes involving H are as follows: H-*supply* is from HOH679 to S3B; the H-*provision* sites are S3B, Fe6, S2B, Fe2, and S2A, between which H atoms can *migrate* and from which H atoms can *add* to the bound substrate or intermediate.

COMPUTATIONAL METHODS

The FeMo-co model used in the density functional calculations includes the essential ligation of all atoms: $-SCH_3$ for cysteine275; glycollate $-OCH_2COO-$ for homocitrate; and imidazole $C_3N_2H_4$ for histidine442. The resting state of the protein corresponds to a charge of −3 for the $Fe_7MoS_9N^c(SCH_3)(OCH_2COO)(C_3N_2H_4)$ model (i.e., $[Fe_7MoN^c]^{18+}$), for reasons already described (*18*). The same net charge of −3 occurs when H atoms, H_2 molecules, and/or neutral substrates are bound to FeMo-co at various mechanistic stages.

Density functional calculations used Delley's program DMol (*50*−*52*), which uses double numerical basis sets with polarization functions ((2005) DMol3, Version MS 3.2, www.accelrys.com/mstudio/ms_modeling/dmol3.html). The calculations are all-electron (477 electrons for the unligated cluster) and spin-unrestricted and use the blyp functional. Other details of the methods and validation data have been reported previously (*30*, *35*). During geometry optimizations, the electron configurations were, in general, uncontrolled and allowed to adopt the orbital occupation and molecular spin that yield lowest energy. FeMo-co and its ligated forms are characterized by a relatively small HOMO−LUMO gap, which means that alternative electronic states are sometimes close in energy, and the ground electronic state can change during an energy minimization. Any such behavior was carefully monitored, principally via the self-consistent field calculations.

Two methods were used to determine transition states (TS) for reaction processes. Where there is no ambiguity about the electronic state, the quadratic synchronous transit method was used, automatically optimizing all geometrical variables in locating the TS. Where control is required to follow the surface of one electronic state for a reaction profile, I manually interpolated the geometry and evaluated the energy and the energy gradient in the determination of the TS. The general procedure was to observe the initial changes in geometry and gradient during small-step energy minimizations from an intermediate geometry and then to use this information to build a new intermediate geometry expected to be just on the other side of the barrier. Iteration of this cycle eventually finds the lowest energy maximum on the reaction coordinate while optimizing all other variables.

RESULTS

Migration of H Atoms. As previously described (*35*), H atoms are supplied to FeMo-co as protons via water molecule HOH679 to the entry point S3B, where each H atom is first bound in conformation S3BH-5; the labeling of the conformations of S3BH is shown in Figure 2. Because it is probable, for most if not all substrates, that some of the H atoms are added to the substrate from atoms on FeMo-co other than S3B, it is necessary for H atoms to migrate to these provider sites. In the previous article, I described the profiles of some of these H migration steps, but because H

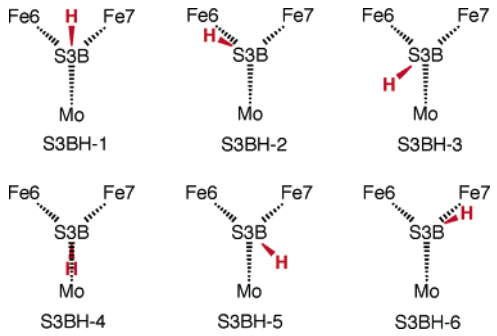

FIGURE 2: Labels for the conformations of S3BH.

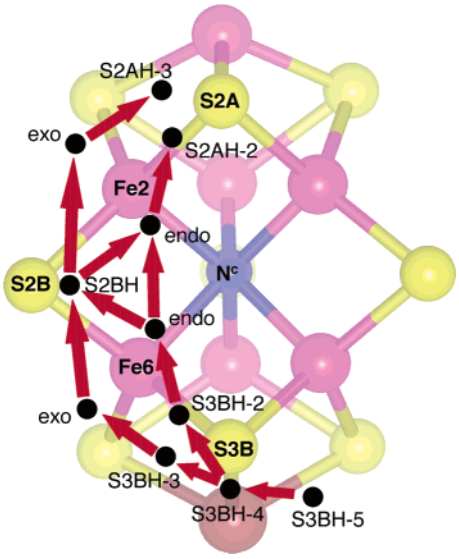

FIGURE 3: Migratory pathway for H atoms to the relevant atoms of FeMo-co from the entry point S3BH-5. The black dots represent local energy minima, and the red arrows are activated migratory processes. Four intermediates have H bound to S3B, two have H bound on Fe6, one has H on S2B, two have H on Fe2, and two have H on S2A.

migration is believed to be a key part of the mechanism, it has been investigated further and with improved accuracy.

The exploration for local energy minima for FeMo-co plus one H atom (i.e., E_1H_1), and the pathways between them, has yielded the results shown in Figure 3. In this and all subsequent figures, the additional ligation of Fe1 and Mo is omitted, and the orientation is that of Figure 1. Starting at the H entry position S3BH-5, the black dots represent the intermediate structures, and the red arrows are activated migratory processes. The structures of the intermediates and the magnitudes of the barriers between them are shown in Figures 4−6.

A number of isomeric conformations exist for S3BH (Figure 4), with variations in the distances from S3B to its surrounding Fe atoms, and variable electronic states. In order for the H atom to move to the Fe6 side of S3B and begin the migration, it must reach S3BH-4, a shallow minimum, against a barrier of 17 kcal mol^{-1}; from S3BH-4 there are negligible barriers for progression to S3BH-2 (in which H bridges S3B and Fe6) or to S3BH-3a with elongated S3B-Fe7. This latter intermediate has a negligible barrier toward the normal S3BH-3 conformer in which Fe6−S3B is elongated.

From the S3BH-2 and S3BH-3 conformers, H migrates to the endo and exo isomers of Fe6-H (Figure 5). S3BH-3

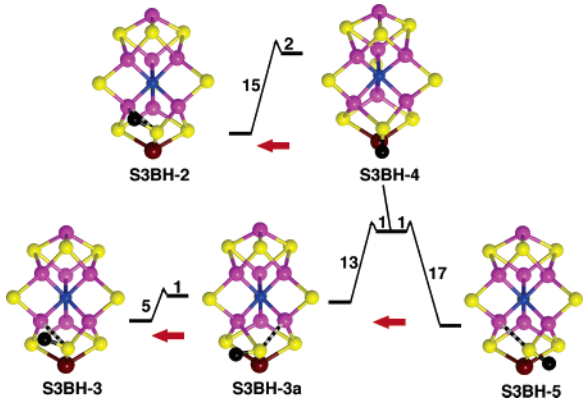

FIGURE 4: Intermediate structures and transition energy (kcal mol^{-1}) profiles for the migration of H atoms (black) from S3BH-5 to conformers S3BH-2 and S3BH-3. The red arrows show the direction of migration, which are right to left to mimic the sense of Figure 3. All species have S = 0. The difference between S3BH-3a and S3BH-3 is a different elongated S3B−Fe bond; the Fe−S bonds marked as broken are in the range 2.5−3 Å.

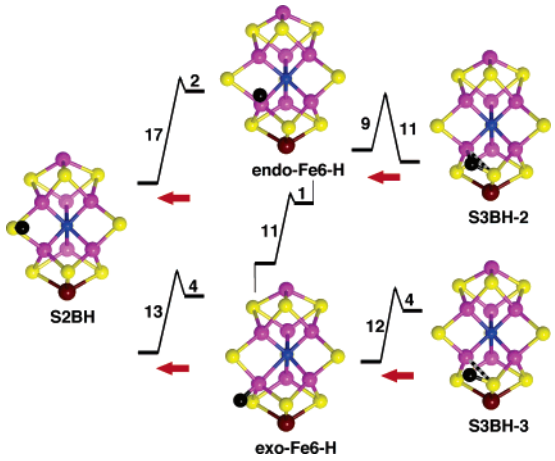

FIGURE 5: Intermediate structures and transition energy (kcal mol^{-1}) profiles for the migration of H from S3BH-2 and S3BH-3 to *endo*- and *exo*-Fe6-H and then to S2BH (all S = 0). The red arrows show the direction of migration. The nonzero (4 kcal mol^{-1}) sum of energy differences among the intermediates *endo*-Fe6-H, *exo*-Fe6-H, and S2BH is due to differences in electronic states.

transforms with a barrier of 4 kcal mol^{-1} to *exo*-Fe6-H, and then with another barrier of 4 kcal mol^{-1}, the H atom moves to S2B. Alternatively, the conformation S3BH-2 can transform against a barrier of 11 kcal mol^{-1} to *endo*-Fe6-H, from which there is a low barrier of 2 kcal mol^{-1} to S2BH. Note that both of these migrations from Fe6-H to S2BH are exergonic. The exergonic (10 kcal mol^{-1}) conversion of *endo*-Fe6-H to *exo*-Fe6-H has a barrier of ca. 1 kcal mol^{-1}.

In the next stage of migration, H moves to Fe2. There are two pathways for H to migrate from the Fe6 domain to the Fe2 domain of FeMo-co. One is directly from the endo coordination at Fe6 to the endo coordination at Fe2 (Figure 3), involving a very shallow intermediate minimum as the Fe2-H-Fe6 bridge; all barriers in this migration are negligible (ca. 1 kcal mol^{-1}). The alternative is from S2BH to either *endo*- or *exo*-Fe2-H, with barriers of 16 and 14 kcal mol^{-1}, respectively (Figure 6). At Fe2, as at Fe6, there is a low barrier (3 kcal mol^{-1}) for the endergonic (11 kcal mol^{-1}) conversion of the endo to exo coordination of H. The barriers for further migration to S2AH conformations are shown in Figure 6.

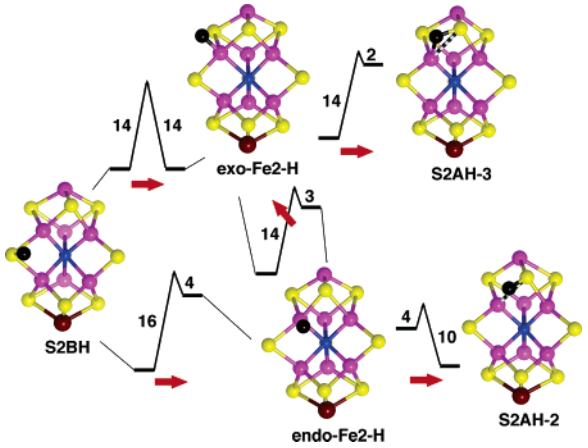

FIGURE 6: Intermediate structures and transition energy (kcal mol^{-1}) profiles for the migration of H from S2BH to *endo*- and *exo*-Fe2-H and then to S2AH conformers (all S = 0). The red arrows show the direction of migration. The barrier for the interconversion of *endo*-Fe2-H and *exo*-Fe2-H is also shown.

In summary, the consequences of these results for the migration of an H atom are (a) the largest barrier (17 kcal mol^{-1}) occurs at the beginning, getting around S3B, but then, barriers of ≤4 kcal mol^{-1} occur for the formation of first, the significant S3BH-2 and S3BH-3 conformers, and then, on to *exo*-Fe6-H and S2BH; (b) the formation of *endo*-Fe6-H involves a larger barrier of 11 kcal mol^{-1}, via either S3BH-2 or *exo*-Fe6-H; (c) H is stabilized on S2B, and barriers of 14 or 16 kcal mol^{-1} occur for migration from S2BH to Fe2-H, but the alternative pathway directly from *endo*-Fe6-H to *endo*-Fe2-H has almost no barrier; (d) the migration from *endo*-Fe2-H to S2AH-2 involves a barrier of only 4 kcal mol^{-1}. Note that the migratory pathway from S3B to S2A via S3BH-2, *endo*-Fe6-H, *endo*-Fe2-H, and S2AH-2 has a maximum barrier of 11 kcal mol^{-1}. Note also that S2BH is a relatively deep well on these energy surfaces, and all pathways out of S2BH have barriers of 13−17 kcal mol^{-1}.

The preceding results describe the locations and migrations of a single H atom on FeMo-co. These are structures for E_1H_1, which is therefore conceptualized not as a single entity but as a sequence of substructures. Then, when a second H atom is introduced at S3BH, it can also migrate to other locations, but the barriers will depend on the location of the first H atom. For example, when the first H atom is already on S2B, the barrier for the S3BH-2 to *endo*-Fe6-H path is 5 kcal mol^{-1}, instead of the 11 kcal mol^{-1} shown in Figure 5. In this way, the E_2H_2 level is viewed as a set of substructures in which the two H atoms may be distributed over the possible sites, with migratory barriers dependent on the distribution. Similar ideas apply to E_3H_3 and E_4H_4.

These E_nH_n intermediates are dynamic states, not necessarily at local equilibrium, because the migration rates need to be considered in the context of other processes that can occur on the full protein scale or at FeMo-co. The crucial process at FeMo-co is the involvement of the substrate. Two key questions arise at this point: how does the substrate bind to FeMo-co, and how does this bound substrate affect the migration of H atoms? In addition, substrate binding is expected to be influenced by the details of the prehydrogenation of FeMo-co. The next two sections describe the main ways in which N_2 and C_2H_2 can bind to FeMo-co.

Binding of N_2 to FeMo-co. There is no experimental data on the structure or dynamics of the binding of N_2 to FeMo-co, but density functional calculations show that N_2 can bind to the central Fe atoms of FeMo-co in a variety of ways. When bound to only one Fe atom, the coordination can be either η^1 (end binding) or η^2 (side bonding), and at each Fe atom, the standard endo and exo coordination positions are available (**1**, **2**). These four coordination modes, when combined with the various numbers and distributions of H atoms on FeMo-co, suggest multiple possible structures for the species $E_3H_3(N_2)$, $E_3H(H_2)(N_2)$, $E_3H(N_2)$, $E_4H_4(N_2)$, $E_4H_2(H_2)(N_2)$, and $E_4H_2(N_2)$ (see Scheme 1) likely to be involved at the initial binding of N_2 to FeMo-co. Many of these possibilities are stable to the dissociation of N_2, but some are not. A representative selection of the stable structures, demonstrating the various geometries for coordination of N_2 at Fe6, classified as *endo*-Fe-η^2-N_2, *exo*-Fe-η^2-N_2, *endo*-Fe-η^1-N_2, and *exo*-Fe-η^1-N_2, is provided in Figure S1 (Supporting Information). *endo*-Fe-η^2-N_2 coordination is unstable to dissociation if there are no H atoms on FeMo-co, but structures combining *endo*-Fe-η^2-N_2 coordination with 1, 2, 3, or 4 H atoms, or 1H + H_2 or 2H + H_2 are stable. An Fe2−H−Fe6 bridge stabilizes Fe-η^2-N_2 coordination. *exo*-Fe-η^2-N_2, *endo*-Fe-η^1-N_2 and *exo*-Fe-η^1-N_2 coordination are stable in the absence of H atoms on FeMo-co and with various combinations of H atoms and H_2 molecules. Tetrahedral, square pyramidal, trigonal bipyramidal, and octahedral coordination stereochemistries at Fe occur in these structures. No instance of N_2 bridging two or more Fe atoms has been found to be stable. Full details of these structures and their stabilities will be published separately.

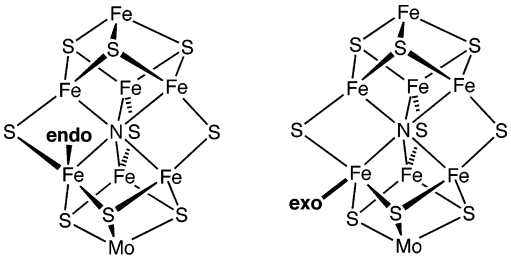

1 endo-coordination at Fe

2 exo-coordination at Fe

In structures with *endo*-Fe-η^1-N_2 coordination, the linear Fe-N-N sequence is directed approximately normal to the FeMo-co face, toward the space occupied by residue 70^{Val}. Potential interference between *endo*-Fe-η^1-N_2 and 70^{Val} has been investigated for structures *endo*-Fe6-η^1-N_2,*exo*-Fe6-H,*exo*-Fe2-H (Figure S1c) and its analogue *endo*-Fe2-η^1-N_2,*exo*-Fe2-H,*exo*-Fe6-H, which are very similar with respect to FeMo-co, but protrude differently into 70^{Val}. Superimposition of the undistorted part of the FeMoc-co framework of either of these structures onto the corresponding atoms of the protein, using methods described previously (*30*), reveals overlap of the distal N atom and the side chain of 70^{Val}. Subsequent energy minimization of the protein structure (with ligated FeMo-co rigid) resolves this conflict by movement of the local helix containing 70^{Val}, indicating that these are strained arrangements. exo-Fe6-η^1-N_2 coordination, tested for structure *exo*-Fe6-η^1-N_2,*endo*-Fe6-H,S3BH-5 (Figure S1d), fits into the surrounding protein making contacts with 191^{Gln} and O1 of homocitrate; these contacts are readily resolved by protein relaxation.

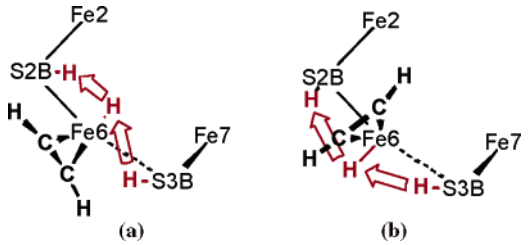

FIGURE 7: Possible but unlikely bypass mechanisms for H migration from S3B to S2B when the substrate C_2H_2 is bound to Fe6.

Binding of C_2H_2 to FeMo-co. A previous article (*30*) modeled the binding of the alkynes propargyl alcohol and propargyl amine ($HC{\equiv}C{-}CH_2OH/NH_2$) at Fe2 and Fe6 of FeMo-co in the 70^{Ala} protein, in the context of modeling the structures of the corresponding alkenes for which there are biochemical and spectroscopic data (*24*, *25*, *29*, *53*). It was concluded that η^2 binding occurred at Fe6 in a conformation intermediate between endo and exo. The possibilities for C_2H_2 binding to hydrogenated FeMo-co, consistent with Scheme 2, have now been explored, and representative structures are presented in Figure S2 (Supporting Information). The full results will be presented in an article on the mechanism of reduction of C_2H_2, but results relevant to questions about H migration are summarized here.

endo-Fe-η^2-C_2H_2 coordination can occur with H atoms on Fe and/or S atoms, and one Fe atom can bind both H in the exo position and C_2H_2 in endo position or H in the endo position and C_2H_2 in the exo position. Fe-η^2-C_2H_2 coordination combined with an Fe2−H−Fe6 bridge is favorable. H atoms on S3B (as S3BH-3) and S2B are well positioned for addition to C_2H_2 coordinated at Fe6. C_2H_2 can bridge two or three Fe atoms, with or without the hydrogenation of Fe.

With this background about the geometrical possibilities for bound substrates N_2 and C_2H_2, I now return to the question of whether bound substrates affect the migration of the H atoms needed for substrate hydrogenation.

Bound Substrates Interfere with H Migration. Substrates bound at Fe6 or Fe2 generally lie in the path of migrating H atoms (Figure 3), and most of the structures for substrates bound at Fe2 or Fe6 would obviously block H migration past these sites. However, because an H atom and a substrate molecule can be bound to the same Fe atom, a bypass mechanism for H migration is a possibility. Structures with *exo*-η^2-substrate and *endo*-H on the same Fe atom could be expected to be the intermediate in H migration between the S atoms on either side of Fe, as illustrated in Figure 7a, and similarly, structures with *endo*-η^2-substrate and *exo*-H on the same Fe might be expected to have an H bypass mechanism (Figure 7b). However, attempts to profile these pathways with density functional calculations revealed large barriers and distortions, in part due to elongated Fe6-N^c in structures with both H and a substrate bound to Fe. Also, at the beginning of migration, the S3BH-3 reactant has elongated Fe6-S3B, and therefore, Fe6 is undercoordinated so that FeMo-co distorts in a way that is not favorable to H-atom transfer, and the substrate impedes the transfer path. Further, if the long Fe-N^c (3.16 Å) in the optimized structure of *endo*-Fe6-C_2H_2,*exo*-Fe6-H (Figure S2a) is shortened in an attempt to improve the geometry for H migration via the *exo*-Fe6-H position (Figure 7b), energy minimization leads instead to the addition of H to C_2H_2.

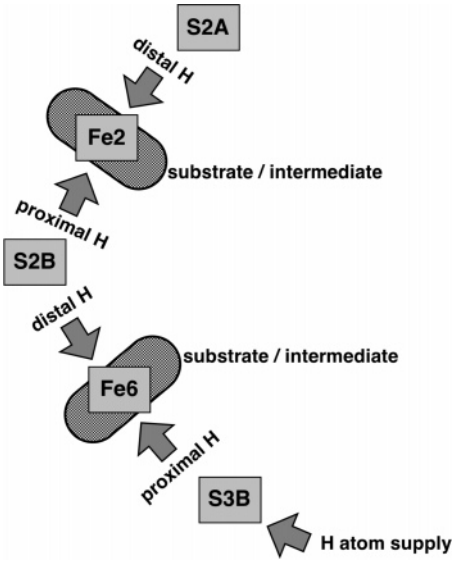

FIGURE 8: General model for the provision of H atoms to substrates or intermediates bound at Fe2 or Fe6 (oval domains). The squares represent the possible locations of H atoms in the reduced states E_nH_n of FeMo-co, all H atoms being initially supplied via S3B. The proximal and distal directions for the addition of H atoms to the substrate at Fe2 or Fe6 are marked.

Structures with substrate and H bound to the same Fe atom may be significant in processes transferring H to substrate, but do not facilitate the passage of the H atom around the substrate. Indeed, the fundamental premise for the mechanism of the catalyzed reduction of substrates at FeMo-co is that substrates are bound at Fe, and the contiguous S atoms gather H atoms that are to be transferred to the substrate. The objective is to add H atoms to the substrate, not pass them around it. The conclusion is that the migration of H atoms past bound substrates is neither possible nor relevant.

General Model for the Hydrogenation of Substrates. The outcome of the foregoing considerations is the general model of Figure 8. The possible domains for the H atoms in the reduced states E_nH_n of FeMo-co are depicted as squares, and the oval domains are the locations of bound substrate or intermediate. Proximal and distal directions for the provision of H atoms to add to substrate are defined. These directions arise because the initial H supply is only from S3B, and H atoms are assumed not to migrate between the proximal and distal providers once the substrate is bound.

If the substrate requires only two H atoms for reduction (e.g., C_2H_2), then it is possible for these to be provided, sequentially, from the proximal providers alone. This would provide a mechanism for the major occurrence (96% in wild type) of cis addition of H atoms to C_2H_2. For the physiological substrate N_2, six H atoms are to be added, and it seems very unlikely that they would all be added by sequential supply from the proximal side without the use of H providers on the distal side of bound N_2 or its intermediates.

The key concept is that H atoms to be added from the distal side need to be positioned prior to substrate binding, whereas H atoms can be continuously supplied from the proximal side.

These concepts aid the understanding of the different reduction levels E_nH_n for initial productive binding of C_2H_2

(at E_1H_1) and N_2 (at E_3H_3). My proposal is that although N_2 is able to bind to FeMo-co at levels less reduced than E_3H_3, three H atoms need to be distally pre-positioned on FeMo-co prior to N_2 binding if there is to be full transfer of H atoms to N_2 and to the N_2H_x and NH_x intermediates leading to product NH_3.

Two-Site Model for the Hydrogenation of C_2H_2. At an increased concentration of C_2H_2, nitrogenase from species *Cp* (*48*) and *Kp* (*47*) exhibits enhanced product formation, consistent with the reaction at two sites, labeled high affinity and low affinity. At pH 7.4, *Av* nitrogenase has diminished production at high concentration of C_2H_2 (i.e., substrate inhibition) (*48*), but at pH 8.2, the reactivity changes to enhanced production and two-site reactivity (*39*) as observed for *Cp* and *Kp*. I propose that Fe6 is the high-affinity site, and Fe2 is the low-affinity site, and that the different experimental kinetic characteristics of these two sites are not due to fundamental differences in their binding of C_2H_2 but to differences in the preparatory location of H atoms on FeMo-co.

Results showing that the differences between the coordination of C_2H_2 at Fe2 and at Fe6 are relatively minor are presented in Figure S3 (Supporting Information). Pairs of structures with *endo*-Fe2-η^2-C_2H_2 or *endo*-Fe6-η^2-C_2H_2 coordination, and related by pseudo reflection between the Fe2 and Fe6 ends of FeMo-co, are seen to have similar structures and similar reaction profiles for the association/dissociation of C_2H_2. These results are consistent with the previously described small differentiation of the Fe1 and Mo ends of FeMo-co (*35*). The differences occur mainly in the long nonbonding Fe-N^c distances and in the relatively large association barriers for C_2H_2 when FeMo-co carries no H atoms (i.e., the E_0 level). Singly and doubly hydrogenated FeMo-co's have diminished barriers for the association of C_2H_2, which is consistent with C_2H_2 binding at the E_1H_1 and E_2H_2 levels (Scheme 2).

My proposal is that the reduction of C_2H_2 at Fe2 differs from that at Fe6 because the preparatory migrations of H atoms require different and additional steps. The hydrogenation of C_2H_2 bound at Fe6 requires H atoms supplied from S3B and/or S2B,Fe6, whereas the hydrogenation of C_2H_2 bound at Fe2 requires H atoms supplied from S2B and/or S2A,Fe2 (Figure 8). Additional migration is required to prepare the H atoms required for the reduction of C_2H_2 bound at Fe2, and the kinetic and/or thermodynamic penalty due to this impairs the reactivity parameters for the Fe2 (low-affinity) site. The kinetic data indicate that the difference between the high- and low-affinity sites for C_2H_2 reaction is in K_m. The present model accounts for these data because preparatory H migration prior to substrate binding, whether under kinetic or equilibrium control, will decrease the effective concentration of the active site and increase the apparent value of K_m. Fe6 is the small K_m site, and Fe2 is the large K_m site.

Along with the additional preparatory H migration steps required for reaction at Fe2, there are differences in the character of the preparatory structures because proximal H provision for Fe6-C_2H_2 involves S3B (μ_3-S), whereas proximal H provision for Fe2-C_2H_2 involves S2B (μ-S), and the H migration profiles above show that the μ_3-S-H and μ-S-H atoms are likely to be available at different chemical potentials.

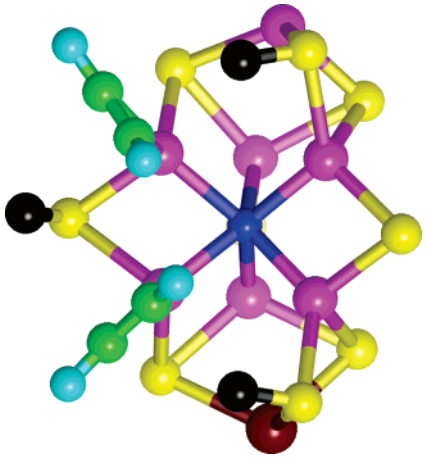

FIGURE 9: Optimized structure with C_2H_2 molecules bound at both Fe2 and Fe6, suggested as an intermediate when reaction is occurring at both the high-affinity (Fe6) and low-affinity (Fe2) sites. Fe2-N^c 2.12 Å; Fe6-N^c 2.07 Å; Fe2-S2A 3.75 Å; and Fe6-S3B 3.71 Å.

The key concept is that Fe2 and Fe6 are approximately equivalent when considered relative to the pseudo reflection plane through the three central μ-S atoms of FeMo-co but are distinctly different when considered in the context of the vectorial migration of H atoms from S3B.

An important question remains. How can binding of C_2H_2 at the low-affinity site Fe2 be inhibitory to the reduction of C_2H_2 at Fe6 in the *Av* protein at pH 7 but be complementary in the *Kp* and *Cp* proteins, and in the *Av* protein at pH 8.2? Although a detailed response is not yet provided, I believe the explanation lies in the variations in C_2H_2 binding around the endo−exo arc of coordination positions at Fe2 and/or Fe6. The actual position of bound C_2H_2 depends on the distribution of H atoms. Although near endo coordination of C_2H_2 at both Fe2 and Fe6 is obviously inhibitory because of steric clash, energy-minimized structures such as that in Figure 9 show how different reactions could occur concurrently at both Fe2 and Fe6 and explain the two-site data. The pH dependence is consistent with the modification of the relevant array of H atoms.

Mutually Inhibitory Reactions of N_2 and C_2H_2 in the Wild-Type Enzyme. The observation to be structurally interpreted is that in the wild-type enzyme N_2 is a weak competitive inhibitor of C_2H_2 reduction, whereas C_2H_2 is a strong noncompetitive inhibitor of the reduction of N_2. It is proposed that the initial binding of N_2 occurs at Fe6, probably with η^2 coordination, forming intermediate structures such as those illustrated in Figure S1. Initial binding of N_2 at Fe2 is postulated to be kinetically less favorable than at Fe6, for reasons of the H preparation penalty similar to those presented in the previous section for C_2H_2, and because N_2 binding is weaker than C_2H_2 binding (from association/dissociation profiles; not shown), the use of Fe2 for the initial binding of N_2 is regarded as insignificant, although Fe2 is likely to be involved with Fe6 in N_2H_x intermediates (see below). Therefore, the competition between N_2 and C_2H_2 occurs at Fe6.

The strong noncompetitive inhibition of N_2 reduction by C_2H_2 occurs because C_2H_2 is relatively strongly bound at Fe6 and blocks the continued migration of H atoms to generate the distal provision sites included in the E_3H_3 and

E_4H_4 levels required for the hydrogenation of N_2. The bound C_2H_2 also consumes two adjacent H atoms as it is reduced. Increase in the concentration of N_2 will cause some of the C_2H_2 to be displaced by N_2 at Fe6, but this will continue to block preparatory H migration. Thus, the competing N_2 is unable to reverse the blockage of H migration around Fe6 caused by C_2H_2 or to restore the preparatory hydrogenation required for the reduction of N_2. This accounts for the noncompetitive character of the inhibition of N_2 by C_2H_2. This interpretation of noncompetitive inhibition involves one binding site rather than the conventional two binding sites and is similar to previous suggestions of two reduction levels at one site (*13*, *14*, *49*, *54*); the new factor here is preparatory H migration, which when blocked, inhibits productive reaction.

The opposite mutual inhibition, that is, weak competitive inhibition of C_2H_2 reduction by N_2, has the standard interpretation in which both substrates compete for the same Fe6 site, and an increase in the concentration of C_2H_2 displaces the inhibitory N_2. H migration is not part of the interpretation of this inhibition.

Reactions of the $^{Gly}69^{Ser}$ Protein. The mutation of *Av* residue α-69 from glycine to serine severely thwarts the reduction of C_2H_2, which is retained only with the low-affinity kinetics of wild-type protein. The reduction of N_2 is unchanged. C_2H_2 still inhibits the reduction of N_2 but with competitive kinetics in contrast to the noncompetitive pattern of wild-type protein.

The structure of the MoFe protein with the $^{Gly}69^{Ser}$ modification is not known, but I have modeled it using force-field methods as previously described (*30*). A good conformation for the CH_2OH side chain involves hydrogen bonds with the carbonyl of 65^{Ala} and water 34, which is further hydrogen bonded to the O2 of homocitrate and to water 185, as detailed in Figure 10. The effects of the protein modification are closest to Fe6 and not near Fe2 or the other Fe atoms. From this, I conclude that the changed reactivities of this modified protein occur at Fe6 and that they are mainly sterically imposed even though the distance between the OH group and Fe6 is 7 Å.

For the α-69^{Ser} protein, I postulate that (a) C_2H_2 is able to bind to Fe6 but that H transfer to Fe6-C_2H_2 is not possible; (b) C_2H_2 retains its normal binding and less efficient reduction at Fe2; and (c) normal binding of N_2 at Fe6 occurs followed by normal hydrogenation. The inhibition of the N_2 reaction by C_2H_2 is caused by reversible C_2H_2 binding to Fe6 with which N_2 can compete. The significant point and difference with wild-type behavior is that C_2H_2 bound at Fe6 does not consume any of the surrounding H atoms, which are therefore available for the competing N_2 reaction. The noncompetitive inhibition of N_2 hydrogenation by C_2H_2 in the wild type occurs because C_2H_2 consumes surrounding H atoms that are therefore not available to N_2; in 69^{Ser}, this consumption of H atoms is blocked. Implicit in this interpretation is noninterference by 69^{Ser} in the other processes involved, namely, H entry and migration, ingress of C_2H_2, and electron transfer. It is reported (*44*) that V_{max} for C_2H_2 reduction in 69^{Ser} is close to that of the wild-type enzyme, which is consistent with the proposed unchanged reactivity at Fe2. The competitive inhibition by N_2 of C_2H_2 reduction (*44*) occurs because N_2 and C_2H_2, binding competitively at Fe6, block the H migration past Fe6 as required for the hydrogenation of C_2H_2 at Fe2.

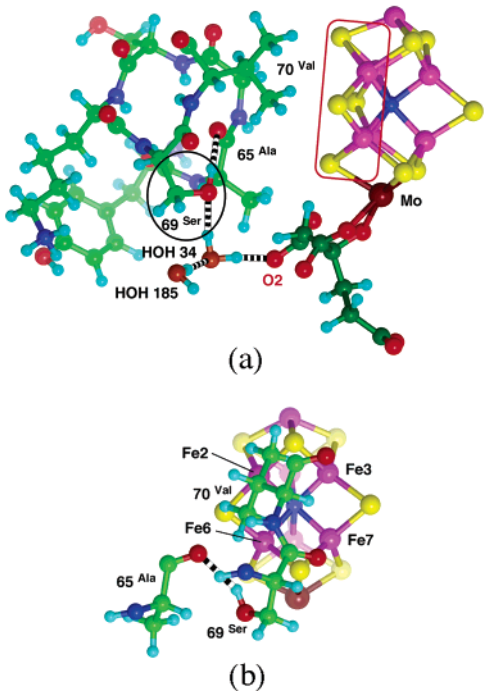

FIGURE 10: Optimized model for the structure of the α-$^{Gly}69^{Ser}$ modification of the MoFe protein (derived from structure 1M1N). (a) Helix from 65 to 70, the hydrogen bond from 69^{Ser} OH to the carbonyl of 65^{Ala}, and the hydrogen bonds that link 69^{Ser} OH to the carboxyl O2 of homocitrate (C atoms, dark green) via water molecule 34, which is also hydrogen bonded to water 185. The 69^{Ser} side chain is enclosed in black, and the relevant Fe2,Fe3,Fe6,Fe7 face of FeMo-co is enclosed in red. (b) Simplified view directly toward the Fe2,Fe3,Fe6,Fe7 face, showing how the 70^{Val} side chain is slightly closer to Fe2, whereas the 69^{Ser} side chain is nearest to Fe6.

The essence of this argument is that the modified surrounding protein blocks H transfer to Fe6-C_2H_2 but not to Fe6-N_2. I believe this occurs because the putative first intermediate in the hydrogenation of bound C_2H_2 projects more into the space toward 69^{Ser} than do the early intermediates in the hydrogenation of N_2. This is supported by my calculations of likely structures for early intermediates. Figure 11 shows the calculated structure of a probable first intermediate Fe6-η^2-C_2H_3 after the transfer of H from S3B in comparison with four calculated structures for the intermediates in the hydrogenation of N_2. The η^2-C_2H_3 group has moved around Fe6 toward the exo position in order that the second H atom can be transferred from S3B to the second C atom, and in so doing, the CH_2 of η^2-C_2H_3 is protruding toward 69^{Ser}. The hydrogenation of bound N_2 is believed to be geometrically different, with the N atoms occupying locations near and between Fe6 and Fe2, as in the possibilities shown in Figure 11b. I propose that because six transfers of H atoms to N atoms are required for the full reduction of N_2, both N atoms need to be kept close to the H provision sites (S3B, Fe6, S2B, Fe2, and S2A) and that Fe2 and Fe6 are both involved in the coordination of the intermediates that remain close to the reaction face. This is fundamentally different from the reduction of C_2H_2, which requires only two H atoms that can be provided to it while it is η^2 bound to only Fe6 and extending away from the reaction face.

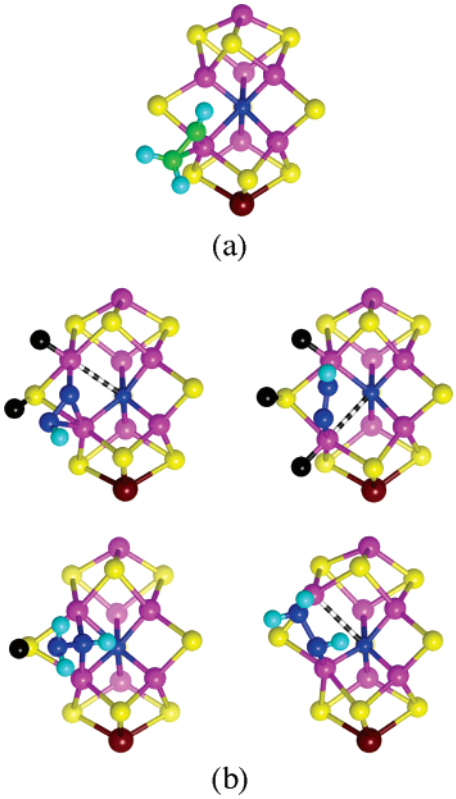

FIGURE 11: Calculated structures for possible intermediates in the hydrogenation of (a) C_2H_2 and (b) N_2. The H atoms bound to the intermediates are cyan, and the H atoms bound to FeMo-co are black.

Residue α-191 is also located in the space exo to Fe6, and an increase in the size of the side chain from glutamine to lysine modifies reactivity. The $^{Gln}191^{Lys}$ mutant is unable to reduce N_2 (*55*), and the K_m for C_2H_2 reduction is increased by a factor of about 70 (*37*). This is consistent with retention of C_2H_2 reactivity only at Fe2. The effect of $^{Gln}191^{Lys}$ mutation is similar to but more drastic than that in $^{Ala}69^{Ser}$, and the structural interpretations are similar.

Kinetics of H Migration. What is required for the rates and the timing of the H migration steps? This question is to be considered in the context of the well-established Thorneley−Lowe description of the sequences of events that generate and use the E_nH_n intermediates. Each cycle (the Fe protein cycle) of reduction of FeMo-co within the MoFe protein, from E_nH_n to $E_{n+1}H_{n+1}$, involves a sequence of three processes: (1) the association of the reduced Fe protein, 2MgATP, and the MoFe protein; (2) the hydrolysis of MgATP and the transfer of one electron from the Fe protein to the MoFe protein; and (3) the dissociation of the reduced MoFe protein and the oxidized Fe protein. This final dissociation of the proteins is rate-determining when all reactants are at saturating concentrations. A key feature of the Thorneley−Lowe simulations is that the association of the Fe protein with the MoFe protein prevents the release of H_2, and it is concluded that the MoFe protein can bind substrates and release products only when it is uncomplexed by the Fe protein (*10*, *11*, *31*).

H migration steps and H transfers to substrate, occurring at the surface of FeMo-co, can be expected to proceed largely independent of the Fe protein cycle. Therefore, I suggest that it is only at the points where FeMo-co receives an electron, binds a substrate (or inhibitor), or releases a product that the timelines for protein events and FeMo-co events need to synchronize. Scheme 3 is a generalized representation of my concept of the timelines for protein events (above the timeline) and FeMo-co events (below the timeline). Once an electron is transferred to FeMo-co, it is assumed that proton supply is relatively fast and that the migration of the H atom generated on S3B occurs on a time scale similar to that of the rate-determining dissociation of the Fe protein. Therefore, each E_nH_n state develops as a migratory sequence of substructures, until it is interrupted by protein events that introduce another electron, allow the release of H_2, or allow the binding of substrate. After substrate binding, the relatively slow transfers of H atoms to the substrate can occur until the next electron injection. Substrate binding and H_2 release, both influence the migratory pathways after the next electron injection.

These concepts are qualitative and speculative at this stage. As specific models for H migration, substrate binding, H transfer to substrate, and dissociation of the product are developed and reaction barriers are calculated, it will be interesting to convert these barriers to rate constants (with assumptions), compare them with the Thorneley−Lowe rate constants, and test them in simulations of the Thorneley−Lowe kinetic data.

Stereoselective Hydrogenation of C_2H_2. The hydrogenation of C_2D_2 by the wild-type enzyme is stereoselective, yielding 96% *cis*-$C_2D_2H_2$ under normal assay conditions (*36*, *39*). With increased pC_2H_2 (> 0.1 atm), where the *Av* MoFe protein shows evidence of substrate inhibition (see above), the proportion of *cis*-$C_2D_2H_2$ decreases to ca. 85% (*39*). The $^{His}195^{Gln}$ mutant protein hydrogenates C_2H_2 with the same kinetic parameters as that of the wild type (*46*) and yields 99% *cis*-$C_2D_2H_2$ (*37*). The $^{Gly}69^{Ser}$ mutant, which hydrogenates C_2H_2 only by the low-affinity pathway, yields 95% *cis*-$C_2D_2H_2$ (*38*). Stereoselectivity decreases to 67% *cis*-$C_2D_2H_2$ in the $^{His}195^{Asn}$ protein, but this mutant has strongly diminished activity (*38*) and EPR intensity (*46*), which raises uncertainty about the significance of the loss of stereoselectivity.

The proposed mechanism in which two H atoms are sequentially transferred from the proximal supply side (S3B-H) to C_2H_2 coordinated around the endo−exo arc at Fe6 readily accounts for the normal cis hydrogenation. Trans hydrogenation can occur if one H atom is added from the distal side (S2B-H) and one from the proximal side (S3B-H). In the 195^{Gln} protein, the hydrogen bond from residue 195 to S2B maintains the correct relative orientation and separation of FeMo-co and the surrounding protein (*46*) but is not part of the H atom transfer. These mechanisms for cis and trans hydrogenation retain two Fe−C bonds until the $C_2D_2H_2$ is formed, after which there is dissociation of product. An alternative mechanism involves the severance of one Fe−C bond after the first H atom transfer to yield a σ-vinyl intermediate, **3**, which my calculations show to undergo exergonic twisting about the C−C bond (Fe−C−C−H changes from ca. 90 to ca. 0°), which can result in loss of stereochemical selectivity because the twisting can occur in either direction prior to the addition of the second H atom. Another mechanism involves Fe−H as the supplier of H, rather than S−H. This also leads to intermediate **3** and loss of stereochemical selectivity. Calculations also

Scheme 3: Comparative Timelines for Events Involving the Proteins (above the timeline) and FeMo-co (below the timeline)[a]

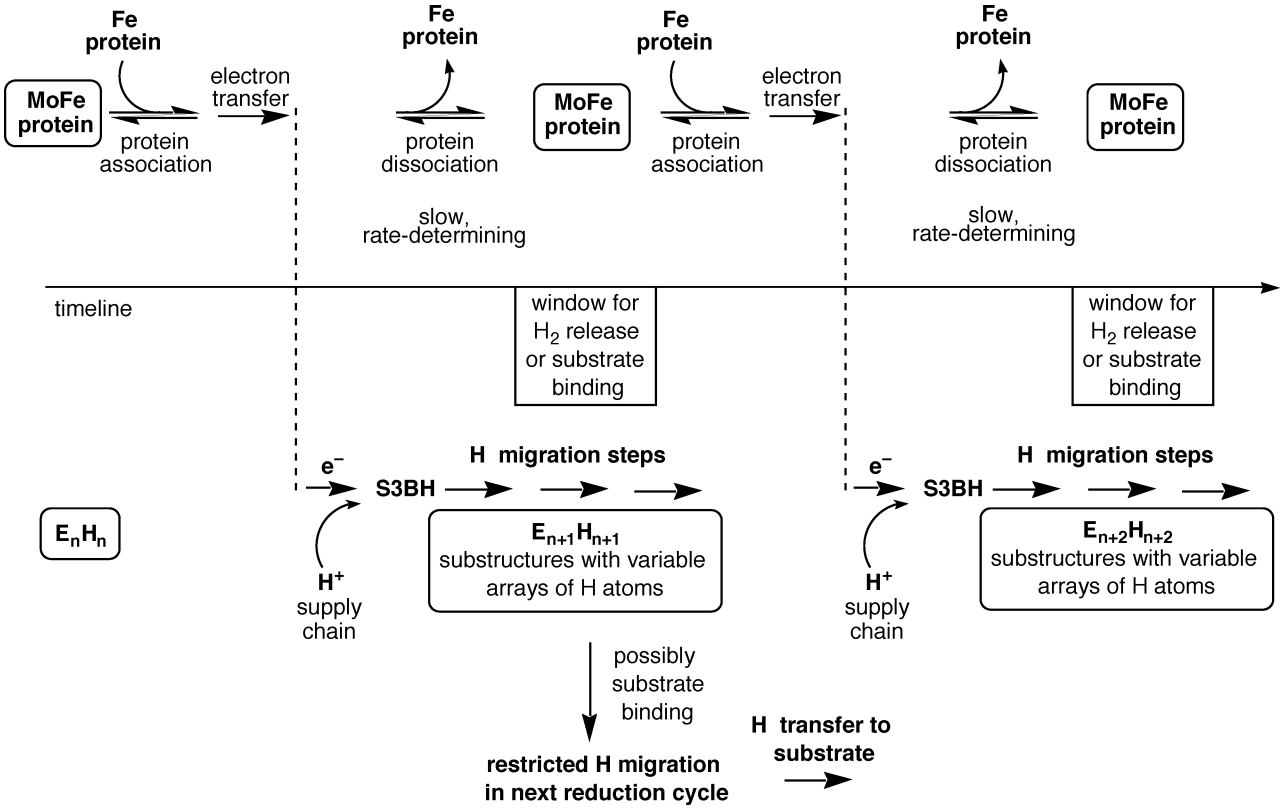

[a] Along the timeline, the synchronization of protein events and Femo-co events occurs where there is electron transfer to FeMo-co (broken line) and where H_2 is released and/or substrates are bound (rectangular box) when the MoFe protein is not complexed with the Fe protein. Each $E_{n+1}H_{n+1}$ generated from E_nH_n is potentially a series of substructures forming in a sequence that could be interrupted at specific times by the dissociation of H_2 or the binding of substrate.

indicate that Fe-H supply can go further and generate intermediates with $CHCH_3$ or CH_2CH_3 σ-bonded to Fe, leading to the production of C_2H_6, which is found to be associated with decreased stereoselectivity in some mutant enzymes (*37*, *38*).

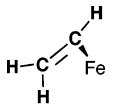

3

In relation to H atom migration, my structural interpretations of the reactivity and stereoselectivity data are as follows. (1) The normal wild type and 195^{Gln} reactions involve two proximal H atom transfers from S3B-H to C_2H_2 coordinated at Fe6. Prior to the coordination of C_2H_2 at Fe6, there is migration of one H atom to S2B; this S2B-H is uninvolved and is the H atom present in the E_1H_1 intermediate after dissociation of product ethylene (Scheme 2). A small proportion of H atom transfers occur from S2B-H rather than from S3B-H, resulting in the $\leq$4% formation of *trans*-$C_2D_2H_2$. (2) The 69^{Ser} reactions involve sequential H atom transfers from S2B-H to C_2H_2 coordinated at Fe2 to yield the predominantly cis product with a small proportion of H transfer from S2A-H or Fe2-H, generating the trans product. This requires that one H atom migrates past Fe6 between the events in which unproductive binding of C_2H_2 at Fe6 and productive binding of N_2 at Fe6 occur, and this impediment contributes to the low reactivity of C_2H_2 in this mutant. (3) At high pC_2H_2, where there is binding at both Fe6 and Fe2 and increased occupancy of the Fe6 site, the preceding mechanism (2) for cis addition at Fe2 is thwarted, and structures such as that in Figure 9 or structures with Fe2-H allow for trans addition, increasing the overall proportion of trans product, as observed. These ideas are being tested by calculations of the relevant reaction profiles.

DISCUSSION

Until recently, the catalyzed reductions effected by nitrogenase have been conceived and discussed in terms of electron transfer to the substrate, which is bound to FeMo-co, followed by protonation of the substrate from nearby proton donors. In the previous article I argued that these nearby residues, particularly α-195^{His} and α-96^{Arg}, function as important hydrogen bonding sites but are unlikely to provide a continuing supply of protons. The continuing proton supply is to S3B, allowing electrons transferred to FeMo-co to be converted to H atoms on S3B, from which these H atoms can migrate to other Fe/S atoms on the active face of FeMo-co. Substrate reduction occurs by transfers of these H atoms to substrates and intermediates bound at FeMo-co; thus, substrate reduction is a process of hydrogenation, rather than sequential electronation and protonation.

The required preparatory H migration is substrate-dependent. In the present article, I have focused on these H migration steps, in relation to substrate binding sites, describing the structures and dynamics of H migration and some stereochemical consequences. This has enabled the development of a mechanistic framework that provides a consistent structural interpretation of many experimental data.

I first summarize the relevant elements of this structural-mechanistic model for nitrogenase.

(1) After electron transfer to FeMo-co, H atoms are generated by fast proton supply to S3B and migrate via several pathways from S3B to locations on the FeMo-co face, specifically Fe6, S2B, Fe2, and S2A. After the initial movement of H around S3B, the activation energies for H migration are estimated to be of the order 5−15 kcal mol^{-1} and no more than 11 kcal mol^{-1} for a complete pathway to S2A. S2B-H is a deeper local energy well, and *exo*-Fe-H is favored over *endo*-Fe-H.

(2) Each of the E_nH_n levels of the Thorneley−Lowe mechanism is potentially a sequence of substructures with different distributions of the H atoms, developing at FeMo-co during and independent of the dissociation of the Fe-protein from the MoFe protein in the Fe-protein cycle.

(3) N_2 and C_2H_2 initially bind at Fe6, whereas C_2H_2 can bind also at Fe2. η^2 coordination near the endo position at Fe is most likely. The coordination of N_2 and C_2H_2 can occur with or without H atoms bound to the S and Fe atoms of the FeMo-co face, that is, at the E_0, E_1H_1, E_2H_2, and E_3H_3 levels, but not all of these are productive or relevant. The dynamics of the coordination of N_2 and C_2H_2 at Fe6 or Fe2 depend on the number and distribution of bound H atoms, providing a mechanism for selection of the actual binding level and geometry.

(4) The reduction of substrates is by transfer of H atoms located at the provision sites, of which S3BH-2, S3BH-3, S2BH, S2AH-2, and S2AH-3 are expected to be favorable, with *endo*-Fe-H and *exo*-Fe-H, and Fe2-H-Fe6 also possible.

(5) The coordination of substrates and intermediates at Fe6 or Fe2 blocks the vectorial H migration past these sites. Proximal and distal directions for H addition to substrates and intermediates are created. After substrate binding, further H atoms for addition to the substrate and its hydrogenated intermediates can be provided only from the proximal direction. The proximal H source for Fe6 is a μ_3-S atom (S3B), whereas the proximal source for Fe2 is μ-S (S2B).

(6) The locations of the H atoms influence substrate binding, and substrate binding influences H atom migration.

(7) Although coordination at Fe2 is only marginally different from the coordination at Fe6, Fe2 is less reactive as a catalytic site than is Fe6 because of the additional preparatory H migration steps required.

(8) The cis addition to C_2H_2 involves two proximal S-H atoms; trans addition to C_2H_2 involves one proximal and one distal S-H atom or may involve Fe-H atoms.

(9) Because six H to N transfers are required for the full reduction of N_2, both N atoms need to be kept near the H provision sites. Intermediates N_2H_x involved in the reduction of N_2 are bound close to Fe6 and Fe2, unlike the intermediates in the reduction of C_2H_2, which are bound to one or the other of the two Fe atoms and can extend further from the reaction face.

This model provides a consistent structural interpretation of many experimental data, summarized as follows.

(a) The two sites at which C_2H_2 reacts in wild-type proteins are Fe6, the high-affinity low K_m site of the literature, and Fe2, the low affinity high K_m site, and the differentiation of these sites is essentially due to the different preparatory H migration required for the reaction at each site. The simultaneous binding of C_2H_2 at both Fe2 and Fe6 as shown in Figure 9 can explain the observed additive reactivity at high pC_2H_2, whereas more *endo*-Fe-C_2H_2 binding at Fe2 and Fe6 can explain the observed substrate inhibition at high pC_2H_2.

(b) The competitive inhibition of C_2H_2 reduction by N_2 in wild type occurs because both substrates compete for the same Fe6 site.

(c) The strong noncompetitive inhibition of N_2 reduction by C_2H_2 in wild type involves only the Fe6 site. C_2H_2 bound at Fe6 blocks the additional H migration required for the 6H hydrogenation of N_2, and consumes 2H in its own reduction. N_2, which displaces C_2H_2, still blocks the required H migration and cannot restore lost H and, therefore, is non competitive with the inhibition by C_2H_2.

(d) The inability of the $^{Gly}69^{Ser}$ mutant to reduce C_2H_2 by the low K_m pathway, while retaining the high K_m pathway and the ability to reduce N_2 as in the wild-type protein, is explained by a structural model for the mutant protein that constricts the reaction space nearest to Fe6. The intermediate C_2H_3 extends away from Fe6 toward the modified protein, whereas N_2H_x intermediates remain close to Fe6 and Fe2; therefore, C_2H_2 hydrogenation is sterically blocked, whereas the hydrogenation of N_2 is not. The reduction of C_2H_2 at Fe2, the high K_m reaction, is not affected by the $^{Gly}69^{Ser}$ modification, which is distant from Fe2.

(e) The competitive inhibition by C_2H_2 of N_2 reduction in the $^{Gly}69^{Ser}$ mutant, contrasting the noncompetitive inhibition in wild-type protein, occurs because C_2H_2 bound at Fe6 in the mutant is unable to consume H atoms that are therefore available to N_2 when it displaces C_2H_2 at Fe6.

(f) The competitive inhibition by N_2 of C_2H_2 reduction in the $^{Gly}69^{Ser}$ mutant occurs because N_2 and C_2H_2, binding competitively at Fe6, block the H migration past Fe6 as required for the hydrogenation of C_2H_2 bound at Fe2.

(g) The diminished reactivity of the $^{Gln}191^{Lys}$ mutant, that is, only the high K_m reduction of C_2H_2 and no reduction of N_2, is believed to be due to the steric blocking of all hydrogenation steps near Fe6 and the retention of only C_2H_2 hydrogenation at Fe2.

(h) Specific H provision sites qualitatively account for the stereoselective hydrogenation of C_2H_2 in the wild type and some mutants and the partial loss of stereoselectivity in other mutants.

This comprehensive model for the reactions of C_2H_2 and N_2 is in part qualitative. The next phase of these investigations includes the calculation of reaction profiles for the possible steps involving the binding of substrates with various H atom distributions, the steps for H transfer to substrates and intermediates, and the dissociation of product. These calculations, in progress, should point to the more probable specific mechanisms. In addition, there are many kinetic and spectroscopic data available on the effects of the strong inhibitor CO to be included in the full model.

Kastner and Blochl have reported calculated mechanisms for the reduction of N_2 and C_2H_2 (*56*−*58*). The Kastner−Blochl mechanism is fundamentally different from my model because it involves severance of a (μ-S)−Fe bond when μ-S is hydrogenated, after which the dangling Fe-SH group moves well away. These authors propose that the substrate binds between the Fe atom with dangling Fe-SH and the Fe atom that has lost μ-S. The possibility of endo coordination of substrates and intermediates, with the retention of the Fe−

(μ-S)−Fe or the Fe−(μ-SH)−Fe bridge, is not mentioned in the articles of Kastner and Blochl. They use NH_4^+ as the artificial proton donor in most steps instead of H atom transfer from adjacent Fe,S atoms. Apart from these chemical differences, I believe that it will be difficult to reconcile the Kastner−Blochl mechanism within the spatial and hydrogen bonding requirements of the surrounding protein.

Finally, I return to the issue of the unproven identity of the central atom and the possibility that it may be carbon rather than nitrogen (the possibility of oxygen is discounted by all theoretical calculations). It is more difficult to chemically rationalize the biosynthesis of FeMo-co if the central atom is carbon rather than nitrogen. I have repeated a number of my calculations of hydrogenated and ligated FeMo-co with C replacing N^c (total electron count unchanged) and found that the results are only marginally different. I expect that the general results and implications of this article will be unchanged, should the central atom be directly identified as carbon.

SUPPORTING INFORMATION AVAILABLE

A selection of optimized structures containing N_2 coordinated to Fe6 of FeMo-co, selected optimized structures for C_2H_2 bound to FeMo-co, and comparisons of the geometrical structures and dissociation/association profiles for η^2-C_2H_2 bound at Fe2 and Fe6. This material is available free of charge via the Internet at http://pubs.acs.org. Cartesian coordinates for all structures and transition states are available from the author.

REFERENCES

1. Burris, R. H. (1991) Nitrogenases, *J. Biol. Chem. 266*, 9339−9342.
2. Burgess, B. K. (1993) Nitrogenase structure, function, and genetics, ACS Symposium Series 535, American Chemical Society, Washington, D.C., pp 145−169.
3. Howard, J. B., and Rees, D. C. (1994) Nitrogenase − a nucleotide-dependent molecular switch, *Annu. Rev. Biochem. 63*, 235−264.
4. Peters, J. W., Fisher, K., and Dean, D. R. (1995) Nitrogenase structure and function: a biochemical-genetic perspective, *Annu. Rev. Microbiol. 49*, 335−366.
5. Eady, R. R. (1996) Structure−Function Relationships of alternative nitrogenases, *Chem. Rev. 96*, 3013−3030.
6. Howard, J. B., and Rees, D. C. (1996) Structural basis of biological nitrogen fixation, *Chem. Rev. 96*, 2965−2982.
7. Seefeldt, L. C., and Dean, D. R. (1997) Role of nucleotides in nitrogenase catalysis, *Acc. Chem. Res. 30*, 260−266.
8. Smith, B. E. (1999) Structure, function, and biosynthesis of the metallosulfur clusters in nitrogenases, *Adv. Inorg. Chem. 47*, 159−218.
9. Dos Santos, P. C., Dean, D. R., Hu, Y., and Ribbe, M. W. (2003) Formation and insertion of the nitrogenase iron-molybdenum cofactor, *Chem. Rev. 104*, 1159−1173.
10. Thorneley, R. N. F., and Lowe, D. J. (1985) Kinetics and mechanism of the nitrogenase enzyme system, in *Molybdenum Enzymes* (Spiro, T. G., Ed.) pp 221−284, Wiley-Interscience, New York.
11. Burgess, B. K., and Lowe, D. J. (1996) Mechanism of molybdenum nitrogenase, *Chem. Rev. 96*, 2983−3011.
12. Rees, D. C., and Howard, J. B. (2000) Nitrogenase: standing at the crossroad, *Curr. Opin. Chem. Biol. 4*, 559−566.
13. Christiansen, J., Dean, D. R., and Seefeldt, L. C. (2001) Mechanistic features of the Mo-containing nitrogenase, *Annu. Rev. Plant Physiol. Plant Mol. Biol. 52*, 269−295.
14. Igarashi, R. Y., and Seefeldt, L. C. (2003) Nitrogen fixation: the mechanism of the Mo-dependent nitrogenase, *Crit. Rev. Biochem. Mol. Biol. 38*, 351−384.
15. Rees, D. C., Tezcan, F. A., Haynes, C. A., Walton, M. Y., Andrade, S., Einsle, O., and Howard, J. A. (2005) Structural basis of biological nitrogen fixation, *Philos. Trans. R. Soc. London, Ser. A 363*, 971−984.
16. Einsle, O., Tezcan, F. A., Andrade, S. L. A., Schmid, B., Yoshida, M., Howard, J. B., and Rees, D. C. (2002) Nitrogenase MoFe-protein at 1.16 Å resolution: a central ligand in the FeMo-cofactor, *Science 297*, 1696−1700.
17. Yang, T.-C., Maeser, N. K., Laryukhin, M., Lee, H.-I., Dean, D. R., Seefeldt, L. C., and Hoffman, B. M. (2005) The interstitial atom of the nitrogenase FeMo-cofactor: ENDOR and ESEEM evidence that it is not a nitrogen, *J. Am. Chem. Soc. 127*, 12804−12805.
18. Dance, I. (2003) The consequences of an interstitial N atom in the FeMo cofactor of nitrogenase, *Chem. Commun.* 324−325.
19. Lovell, T., Liu, T., Case, D. A., and Noodleman, L. (2003) Structural, spectroscopic, and redox consequences of a central ligand in the FeMoco of nitrogenase: a density functional theoretical study, *J. Am. Chem. Soc. 125*, 8377−8383.
20. Cao, Z. X., Jin, X., and Zhang, Q. N. (2005) Density functional study of the structure of the FeMo cofactor with an interstitial atom and homocitrate ligand ring opening, *J. Theor. Comput. Chem. 4*, 593−602.
21. Mayer, S. M., Niehaus, W. G., and Dean, D. R. (2002) Reduction of short chain alkynes by a nitrogenase α-70Ala-substituted MoFe protein, *J. Chem. Soc., Dalton Trans.* 802−807.
22. Barney, B. M., Igarashi, R. Y., Dos Santos, P. C., Dean, D. R., and Seefeldt, L. C. (2004) Substrate interaction at an iron-sulfur face of the FeMo-cofactor during nitrogenase catalysis, *J. Biol. Chem. 279*, 53621−53624.
23. Dos Santos, P. C., Igarashi, R., Lee, H.-I., Hoffman, B. M., Seefeldt, L. C., and Dean, D. R. (2005) Substrate interactions with the nitrogenase active site, *Acc. Chem. Res. 38*, 208−214.
24. Benton, P. M. C., Laryukhin, M., Mayer, S. M., Hoffman, B. M., Dean, D. R., and Seefeldt, L. C. (2003) Localization of a substrate binding site on the FeMo-cofactor in nitrogenase: trapping propargyl alcohol with an α-70-substituted MoFe protein, *Biochemistry 42*, 9102−9109.
25. Lee, H.-I., Igarashi, R., Laryukhin, M., Doan, P. E., Dos Santos, P. C., Dean, D. R., Seefeldt, L. C., and Hoffman, B. M. (2004) An organometallic intermediate during alkyne reduction by nitrogenase, *J. Am. Chem. Soc. 126*, 9563−9569.
26. Igarashi, R. Y., Laryukhin, M., Dos Santos, P. C., Lee, H.-I., Dean, D. R., Seefeldt, L. C., and Hoffman, B. M. (2005) Trapping H-bound to the nitrogenase FeMo-cofactor active site during H_2 evolution: characterization by ENDOR spectroscopy, *J. Am. Chem. Soc. 127*, 6231−6241.
27. Barney, B. M., Yang, T.-C., Igarashi, R., Dos Santos, P. C., Laryukhin, M., Lee, H.-I., Hoffman, B. M., Dean, D. R., and Seefeldt, L. C. (2005) Intermediates trapped during nitrogenase reduction of N═N, CH_3−N═NH, and H_2N−NH_2, *J. Am. Chem. Soc. 127*, 14960−14961.
28. Barney, B. M., Laryukhin, M., Igarashi, R. Y., Lee, H.-I., Dos Santos, P. C., Yang, T.-C., Hoffman, B. M., Dean, D. R., and Seefeldt, L. C. (2005) Trapping a hydrazine reduction intermediate on the nitrogenase active site, *Biochemistry 44*, 8030−8037.
29. Igarashi, R., Dos Santos, P. C., Niehaus, W. G., Dance, I. G., Dean, D. R., and Seefeldt, L. C. (2004) Localization of a catalytic intermediate bound to FeMo-cofactor of nitrogenase, *J. Biol. Chem. 279*, 34770−34775.
30. Dance, I. (2004) The mechanism of nitrogenase. Computed details of the site and geometry of binding of alkyne and alkene substrates and intermediates, *J. Am. Chem. Soc. 126*, 11852−11863.
31. Lowe, D. J., and Thorneley, R. N. F. (1984) The mechanism of klebsiella pneumoniae nitrogenase action. Pre-steady-state kinetics of H_2 formation, *Biochem. J. 224*, 877−886.
32. Thorneley, R. N. F., and Lowe, D. J. (1984) The mechanism of klebsiella pneumoniae nitrogenase action. Pre-steady-state kinetics of an enzyme-bound intermediate in N_2 reduction and of NH_3 formation, *Biochem. J. 224*, 887−894.
33. Lowe, D. J., and Thorneley, R. N. F. (1984) The mechanism of klebsiella pneumoniae nitrogenase action. The determination of rate constants required for the simulation of the kinetics of N_2 reduction and H_2 evolution, *Biochem. J. 224*, 895−901.
34. Thorneley, R. N. F., and Lowe, D. J. (1984) The mechanism of klebsiella pneumoniae nitrogenase action. Simulation of the dependences of H_2-evolution on component-protein concentration and ratio and sodium dithionite concentration, *Biochem. J. 224*, 903−909.
35. Dance, I. (2005) The hydrogen chemistry of the FeMo-co active site of nitrogenase, *J. Am. Chem. Soc. 127*, 10925−10942.

36. Dilworth, M. J. (1966) Acetylene reduction by nitrogen fixing preparations from *Clostridium pasteurianum*, *Biochim. Biophys. Acta 127*, 285−294.
37. Fisher, K., Dilworth, M. J., Kim, C.-H., and Newton, W. E. (2000) *Azotobacter vinelandii* nitrogenases containing altered MoFe proteins with substitutions in the FeMo-cofactor environment: effects on the catalyzed reduction of acetylene and ethylene, *Biochemistry 39*, 2970−2979.
38. Benton, P. M. C., Christiansen, J., Dean, D. R., and Seefeldt, L. C. (2001) Stereospecificity of acetylene reduction catalyzed by nitrogenase, *J. Am. Chem. Soc. 123*, 1822−1827.
39. Han, J., and Newton, W. E. (2004) Differentiation of acetylene-reduction sites by stereoselective proton addition during *Azotobacter vinelandii* nitrogenase-catalyzed C_2D_2 reduction, *Biochemistry 43*, 2947−2956.
40. Lowe, D. J., Fisher, K., and Thorneley, R. N. F. (1990) Klebsiella pneumoniae nitrogenase. Mechanism of acetylene reduction and its inhibition by carbon monoxide, *Biochem. J. 272*, 621−625.
41. McLean, P. A., True, A., Nelson, M. J., Lee, H.-I., Hoffman, B. M., and Orme-Johnson, W. H. (2003) Effects of substrates (methyl isocyanide, C_2H_2) and inhibitor (CO) on resting-state wild-type and NifV Klebsiella pneumoniae MoFe proteins, *J. Inorg. Biochem. 93*, 18−32.
42. Rivera-Ortiz, J. H., and Burris, R. H. (1975) Interactions among substrates and inhibitors of nitrogenase, *J. Bacteriol. 123*, 537−545.
43. Hwang, J. C., Chen, C. H., and Burris, R. H. (1973) Inhibition of nitrogenase-catalyzed reactions, *Biochim. Biophys. Acta 292*, 256−270.
44. Christiansen, J., Cash, V. L., Seefeldt, L. C., and Dean, D. R. (2000) Isolation and characterisation of an acetylene-resistant nitrogenase. *J. Biol. Chem. 275*, 11459−11464.
45. Christiansen, J., Seefeldt, L. C., and Dean, D. R. (2000) Competitive substrate and inhibitor interactions at the physiologically relevant active site of nitrogenase, *J. Biol. Chem. 275*, 36104−36107.
46. Kim, C. H., Newton, W. E., and Dean, D. R. (1995) Role of the MoFe protein alpha subunit histidine-195 residue in FeMo-cofactor binding and nitrogenase catalysis, *Biochemistry 34*, 2798−2808.
47. Lowe, D. J., Eady, R. R., and Thorneley, R. N. F. (1978) Electron-paramagnetic resonance studies on nitrogenase of Klebsiella pneumoniae, *Biochem. J. 173*, 277−290.
48. Davis, L. C., Henzl, M. T., Burris, R. H., and Orme-Johnson, W. H. (1979) Iron-sulfur clusters in the molybdenum−iron protein component of nitrogenase. Electron paramagnetic resonance of the carbon monoxide inhibited state, *Biochemistry 18*, 4860−4869.
49. Shen, J., Dean, D. R., and Newton, W. E. (1997) Evidence for multiple substrate-reduction sites and distinct inhibitor-binding sites from an altered azotobacter vinelandii nitrogenase MeFe protein, *Biochemistry 36*, 4884−4894.
50. Delley, B. (1990) An all-electron numerical method for solving the local density functional for polyatomic molecules, *J. Chem. Phys. 92*, 508−517.
51. Delley, B. (1995) DMol, a standard tool for density functional calculations: review and advances, in *Modern Density Functional Theory: A Tool for Chemistry* (Seminario, J. M., and Politzer, P., Eds.) pp 221−254, Elsevier, Amsterdam, The Netherlands.
52. Delley, B. (2000) From molecules to solids with the DMol3 approach, *J. Chem. Phys. 113*, 7756−7764.
53. Lee, H.-I., Benton, P. M. C., Laryukhin, M., Igarashi, R. Y., Dean, D. R., Seefeldt, L. C., and Hoffman, B. M. (2003) The Interstitial atom of the nitrogenase FeMo-Cofactor: ENDOR and ESEEM show it is not an exchangeable nitrogen, *J. Am. Chem. Soc. 125*, 5604−5605.
54. Davis, L. C., and Wang, Y.-L. (1980) In vivo and in vitro kinetics of nitrogenase, *J. Bacteriol. 141*, 1230−1238.
55. Fisher, K., Dilworth, M. J., and Newton, W. E. (2000) Differential effects on N_2 binding and reduction, HD formation, and azide reduction with α-195^{His}- and α-191^{Gln}-substituted MoFe proteins of *Azotobacter vinelandii* nitrogenase, *Biochemistry 39*, 15570−15577.
56. Kastner, J., and Blochl, P. E. (2005) Towards an understanding of the workings of nitrogenase from DFT calculations, *ChemPhysChem 6*, 1−4.
57. Kastner, J., Hemmen, S., and Blochl, P. E. (2005) Activation and protonation of dinitrogen at the FeMo cofactor of nitrogenase, *J. Chem. Phys. 123*, 074306.
58. Kastner, J., and Blochl, P. E. (2005) Model for acetylene reduction by nitrogenase derived from density functional theory, *Inorg. Chem. 44*, 4568−4575.

BI052217H